Flash Sintering of a Three-Phase Alumina, Spinel, and Yttria-Stabilized Zirconia Composite

David Kok[†], Shikhar Krishn Jha[‡], Rishi Raj[‡], Martha Mecartney[†]

[†]Department of Chemical Engineering and Material Science, University of California, Irvine

[‡]Department of Mechanical Engineering, University of Colorado at Boulder

Abstract

Three-phase ceramic composites constituted from equal volume fractions of α-Al_2O_3, $MgAl_2O_4$ spinel and cubic 8 mol% Y_2O_3-stabilized ZrO_2 (8YSZ) were flash-sintered under the influence of DC electric fields. The temperature for the onset of rapid densification (flash sintering) was measured using a constant heating rate at fields of 50-500 V/cm. The experiments were carried out by heating the furnace at a constant rate. Flash sintering occurred at a furnace temperature of 1350°C at a field of 100 V/cm, which dropped to 1150°C at a field of 500 V/cm. The sintered densities ranged from 90-96%. High fields and low current density led to an apparent reduction in the average grain size from 650 nm to 470 nm, due to the lowering of the flash temperature. During flash sintering, alumina reacted with the spinel phase to form a high-alumina spinel solid solution, identified by electron dispersive spectroscopy and from a decrease in the spinel lattice parameter as measured by X-ray diffraction. It is proposed that the solid solution reaction was promoted by a combination of electrical field and Joule heating.

Introduction

Multiphase ceramics may be used to achieve a combination of properties that are not possible in single phase materials. For example, the thermal conductivity of UO_2 can be enhanced by the

addition of alumina, spinel or silicon carbide, thereby imparting stability and high efficiency to nuclear fuels.[1] Multiphase ceramics can have a finer grain size than their single phase constiutents.[2] A fine grain size in nuclear fuels improves radiation damage tolerance [3, 4] and promotes superplastic behavior which can alleviate cracking due to swelling.[5–7]

Recently, the application electrical fields have been shown to accelerate sintering at low temperatures by a process known as *flash-sintering*.[8–13] In this method densification occurs in mere seconds at a certain combination of temperature and electric field. This "flash" sintering is accompanied by a non-linear increase in conductivity.[8] The process is described by three distinct stages.[13] A pre-flash incubation period (Stage 1) is followed by rapid densification and increased conductivity (Stage II), and finally, a quasi-steady-state, current-controlled state called Stage III is established. Sintering can also be enhanced at lower applied fields, without the abrupt nature of flash sintering; this phenomenon has been called *fast-sintering*.[10, 13]

While the temperature for the onset of flash sintering depends on the applied field, the final density depends on the current flowing through the specimen.[11, 14] A higher current setting in Stage II and Stage III increases the final density. In-situ X-ray diffraction (XRD) experiments have shown that flash sintering can also increase the kinetics of phase reaction between different phases and promote new phase formation.[15] The mechanisms for flash and fast sintering are still controversial; Joule heating and the generation of Frenkel pairs are the two main concepts discussed in the literature.[10, 16–19]

In the present experiments, a three-phase system constituted from alumina, spinel and 8YSZ is explored as a pathway for creating fine-grained structures for nuclear fuels. Here 8YSZ serves as an isostructural surrogate for UO_2. On their own, pure alumina does not exhibit flash sintering even at fields of 1000 V/cm, cubic 8YSZ responds favorably to flash sintering with a

threshold of only 15-30 V/cm,[9, 10] while $MgAl_2O_4$ spinel only flashes at high fields of 1000 V/cm.[20]

Materials and Experimental Procedure

Starting powders of cubic 8YSZ (TZ-8YS, Tosoh USA, Grove City, OH), spinel (S30CR, Baikowski, Charlotte, NC) and alumina (TM-DAR, Taimicron, Japan), in equal volume percent (molar ratio 0.42:0.23:0.35 respectively), were attrition milled (HD-01, Union Process, Akron, OH) with 0.5mm high wear resistant zirconia grinding media (YTZ Grinding Media, Tosoh, Grove City, OH) for 8 hours at 600 rpm with isopropyl alcohol in a Teflon coated tank using a YTZ milling arm to ensure a homogenous mixture. The ratio of media to powder was kept to 1 kg of media to 35 g of powder. Equal volume fraction of each starting powder was used to promote interphase-interfaces and to limit grain growth. 2.5 wt % of polyvinyl alcohol binder (Sigma-Aldrich, St. Louis, MO) was dissolved in 100 mL of water and added to make a slurry that was dried at 100°C overnight. The dried slurry was sieved to 106 μm. The mixed powder was uniaxially pressed at 300MPa into dog bone-shaped samples with a green body density of 52% ± 2%. The dog bone samples were made with holes at each end with a gage length of 20 mm, and a cross section of approximately 3.5 mm x 1.3 mm.

Experiments were carried out in a vertical tube furnace with the samples suspended inside the tube furnace with platinum wires hooked onto the holes at the ends of the dog bone samples[13]. The ends were lightly coated with platinum paste to ensure a good electrical contact. Voltage was applied though platinum wires to the sample from a DC high voltage power supply (KL Series, Glassman High Voltage, High Bridge, NJ); voltage and current were controlled a computer and measured with a digital multimeter (Model 2000, Keithley, Cleveland, OH). A

CCD camera with an optical filter was used to take images during the sintering process to measure sample shrinkage.

The sample was held at 600°C for 1 hour to burn out the binder. Next the electric field was applied and the furnace was heated at a constant rate of 10°C/min. The flash was signaled by a rapid increase in conductivity and the power supply was switched to current control when the current reached a preset limit (called Stage II). The sample establishes a quasi-steady state of flash under current control (Stage III); this state was held for 30 seconds, when power was turned off and the furnace allowed to cooled down. Current limit values were selected from experience with flash sintering experiments with other oxides.[18]

The final density of sintered samples was measured using the Archimedes method. Gauge sections of sintered samples (between the two electrode ends) were polished and thermally etched at 1150°C for 30 minutes (or 1100°C for 30 minutes for samples flash sintered at 1150°C) and coated with iridium for SEM analysis. Grain size analysis and microstructure characterization was conducted using SEM/EDS (FEI Magellan XHR SEM, Hillsboro, OR with Oxford EDS Detector, United Kingdom) and XRD (Rigaku SmartLab XRD, Japan).

Results and Discussion

The linear shrinkages under different applied DC voltages with a current limit of 25 mA/mm^2 are shown in Fig. 1. The field and current conditions, the sintering temperature, the final density, and the final grain size are summarized in Table 1. The flash temperature decreases with higher applied electric field, consistent with earlier experience.[14]

Conventional sintering, without an applied field shows that sintering progresses to only 74% density even at 1450°C. At low applied fields, for example 50 V/cm, a resultant density of

95% is obtained. At 100 V/cm sintering occurs partially in the flash mode, reaching a final density of 96%. At 250-500 V/cm, the abrupt onset of densification, which is a feature of flash sintering, can be seen. At 250 V/cm, the sample densifies within seconds at 1230°C with a density of 94%. At 500 V/cm flash sintering occurs at 1150°C with a final density of 90%. The actual sample temperature can be higher than the furnace temperature due to the power dissipated in the sample. The calculated sample temperature in Table 1 was derived from a model that relates the specimen temperature to power dissipation and black body radiation. The validity of this model has been confirmed by *in-situ* measurements of thermal expansion at the Advanced Photon Source.[15, 16]

The power dissipation is calculated from the product of the applied electric field (V/cm) and current density (mA/mm^2). It is plotted as a function of furnace temperature in an Arrhenius plot in Fig. 2. The three stages of flash sintering are represented on this plot. The linear power increase (corresponding to the activation energy) represents Stage I. The abrupt rise in power dissipation signals the onset of the flash, or Stage II. Finally, Stage III is the shown by the quasi-steady state under current control; it was briefly held for 30 seconds and then the power to the specimen was turned off. It is interesting to note that the flash transition occurs within a narrow range of power dissipation, about 6-20 mW/mm^3, for all cases. This range of power density for the onset of the flash is consistent with previous results reported by Cologna et al.[9] on 8YSZ and Naik et al.[13] on 3YSZ-alumina composites. In fact, for wide range of oxides, the onset of flash sintering is in a narrow range between 8 and 30 mW/mm^3.[18]

The ability of flash sintering to quickly densify these samples at low temperatures should result in limited grain growth in the final microstructures of the samples. [21–23] Scanning electron micrographs of the composites sintered under different applied electric fields are shown in Fig. 3.

The darkest gray grains correspond to spinel, medium gray is alumina, and the light gray corresponds to 8YSZ. An average grain size is lowest for the highest field: 470 nm at a field of 500 V/cm and a current limit of 25 mA/mm^2.

A higher current limit of 75 mA/mm^2 and 250 V/cm resulted in a very large grain size of 1.5 μm. At the same time alumina is absent in this specimen suggesting its dissolution into the spinel phase as solid solution. X-ray diffraction data shown in Fig. 4 compare the results for the specimens obtained without the electric field as well as those sintered with 250 V/cm at 25 mA/mm^2 and at 75 mA/mm^2. At 75 mA/mm^2 the diffraction peaks from alumina are missing. The corresponding microstructure shown in Fig. 3(f) also shows the absence of alumina grains. This composite is now approximately 1/3 8YSZ and 2/3 spinel. Fig. 5 shows that the XRD peaks from the spinel phase are systemically shifted to higher 2θ angles, which indicates a reduction of the lattice spacing in the spinel crystal structure expected in non-stoichiometric spinel solid solution when Mg^{2+} is replaced by Al^{3+}. [24] Table 2 also shows that in instances where the alumina is retained, the lattice parameter for spinel remained essentially unchanged. Fig. 6 shows the relationship between Al/Mg ratio and the lattice parameter determined by XRD.

The Al/Mg ratio in the spinel grains was measured by EDS analysis of all samples. EDS analysis on conventionally sintered single-phase spinel using the same powders as for the three phase samples, shows that the starting spinel was close to being stoichiometric, MgO•1.1 Al_2O_3. For conventionally sintered single-phase spinel, the lattice parameter as measured by XRD matches the PDF file 00-021-1152.[25] The conventionally sintered three-phase material has a slight increase in the Al/Mg ratio, MgO•1.5 Al_2O_3. which could be due to dissolution of alumina in the spinel after sintering for 12 hours at the high temperature of 1500°C. Under 250 V/cm at 25 mA/mm^2 the spinel composition deviates significantly from the starting nearly stoichiometric

composition; it is now MgO•1.8 Al_2O_3. At a current density of 75 mA/mm^2 the composition is further enriched in alumina to MgO•3.1 Al_2O_3. The decrease in lattice parameter of spinel with higher alumina content (Fig. 6) correlates with the EDS measurements and with higher current density. However, the case of 500 V/cm at 25 mA/mm^2 is an exception since here the Al/Mg ratio and the spinel lattice parameter is observed to decrease relative to 250 V/cm at 25 mA/mm^2, which may be a result of the much lower flash temperature at this field.

The phase diagram in Fig. 7 shows that the solubility of alumina in spinel increases with temperature.[26] Accordingly, from thermodynamic equilibrium the spinel composition is expected to be MgO•1.5Al_2O_3 at 1500°C, which matches the composition measured in the conventionally sintered specimen that had been held for 5 hours at 1500ºC. In contrast, for the case of 250 V/cm and 25 mA/mm^2, where the specimen temperature during the flash is estimated to be only 1390ºC, EDS analysis yields a much higher alumina content, MgO•1.8 Al_2O_3.

At 250 V/cm and 75 mA/mm^2, when the calculated temperature of the specimen would have reached 1500°C but for only 30 seconds, the spinel composition is MgO•3Al_2O_3, which is hugely different than the prediction from the phase diagram. The phase diagram predicts this composition of the solid solution to be possible only at 1700ºC. If all the alumina is consumed to produce a non-stoichiometric spinel, this would correspond to an Al_2O_3/MgO molar ratio of 0.80/0.20 on the phase diagram in Fig. 7 with a single-phase spinel conversion temperature of 1800°C. Therefore, we attribute the formation of single phase spinel at a sample temperature of 1500ºC within 30 seconds to the electric field.

The spinel microstructure in Fig. 3(f) has some features reminiscent of a melt, but according to the phase diagram melting would require temperatures above 2000°C. Supplementary information (**S1**) appended to this article shows videos comparing the different

field and current conditions shows that the high power density sample deforms extensively during flash sintering. Enhanced creep is expected under high electric fields[27] but creep due to intergranular liquid phase formation should also be considered. Eutectic liquid phases can form at high temperatures (≥ 1715°C for Al_2O_3-Y_2O_3-ZrO_2[28] and ≥ 1807°C for Al_2O_3-MgO-ZrO_2[29]). However, no pockets of residual amorphous intergranular phases were observed. It is possible that there were some loss of MgO from the spinel[30] during flash sintering in the sample where only solid solution spinel was found but no alumina phase, since the measured composition of MgO•3.1 Al_2O_3, corresponds to Al_2O_3 molar fraction of 0.76, whereas the starting powders contained 0.80 molar Al_2O_3.

In-situ XRD synchrotron studies are planned to characterize high temperature reactions in multi-phase systems to better distinguish between the contribution of electric field and Joule heating in the formation of the solid solution spinel during flash sintering.

Conclusions

Flash sintering of a three-phase composites constituted from equal volume fractions of alumina, spinel, and 8YSZ under a DC electric field produced samples with > 90% density in a few seconds at furnace temperatures of 1150-1430°C. The temperature for flash sintering fell from 1350 to 1150°C as the electric field was increased from 100 V/cm to 500 V/cm. The transition to flash occurred at a power density of 6-20 mW/mm^3 regardless of the electric field. Higher fields led to a smaller grain size by lowering the flash temperature; an average grain size of 470 nm at a field of 500 V/cm and current density of 25 mA/mm^2 was obtained. Increasing the power density to 600 mW/mm^3 by increasing the current density to 75 mA/mm^2 at a field of 250 V/cm resulted

in dramatic grain growth as well as the dissolution of alumina to form a solid solution of spinel of composition $MgO•3Al_2O_3$ in just 30 seconds.

Acknowledgements

This material is based in part upon work supported by the Department of Energy under Award Number DE-NE0000711. This report was prepared as an account of work sponsored by an agency of the United States Government. Neither the United States Government nor any agency thereof, nor any of their employees, makes any warranty, express or implied, or assumes any legal liability or responsibility for the accuracy, completeness, or usefulness of any information, apparatus, product, or process disclosed, or represents that its use would not infringe privately owned rights. Reference herein to any specific commercial product, process, or service by trade name, trademark, manufacturer, or otherwise does not necessarily constitute or imply its endorsement, recommendation, or favoring by the United States Government or any agency thereof. The views and opinions of authors expressed herein do not necessarily state or reflect those of the United States Government or any agency thereof. SEM, EDS and XRD work was performed at the UC Irvine Materials Research Institute (IMRI). DK acknowledges support from a US Department of Education Graduate Assistantships in Areas of National Need (GAANN) Fellowship. RR and SKJ at the University of Colorado Boulder gratefully acknowledge support from the Army Research Office under grant No. ARO 69028-MS.

References

[1] J.P. Angle, A.T. Nelson, D. Men, and M.L. Mecartney, "Thermal measurements and computational simulations of three-phase (CeO_2–$MgAl_2O_4$–$CeMgAl_{11}O_{19}$) and four-phase (3Y-TZP–Al_2O_3–$MgAl_2O_4$–$LaPO_4$) composites as surrogate inert matrix nuclear fuel," *J. Nucl. Mater.*, **454** [1–3] 69–76 (2014).

[2] B.N. Kim, K. Hiraga, K. Morita, and Y. Sakka, "A high-strain-rate superplastic ceramic," *Nature*, **413** [6853] 288–291 (2001).

[3] S. Dey, J.W. Drazin, Y. Wang, J.A. Valdez, T.G. Holesinger, B.P. Uberuaga, and R.H.R. Castro, "Radiation Tolerance of Nanocrystalline Ceramics: Insights from Yttria Stabilized Zirconia," *Sci. Rep.*, **5** 7746 (2015).

[4] T.D. Shen, S. Feng, M. Tang, J.A. Valdez, Y. Wang, and K.E. Sickafus, "Enhanced radiation tolerance in nanocrystalline MgGa2O4," *Appl. Phys. Lett.*, **90** [26] 263115 (2007).

[5] T. Chen and M.L. Mecartney, "Superplastic compression, microstructural analysis and mechanical properties of a fine grain three-phase alumina–zirconia–mullite ceramic composite," *Mater. Sci. Eng. A*, **410–411** 134–139 (2005).

[6] C.M. Hoo, D. Men, L. Taherabadi, and M.L. Mecartney, "Grain-Boundary Sliding in a Superplastic Three-Phase Alumina–Zirconia–Mullite Ceramic Composite," *J. Am. Ceram. Soc.*, **94** [7] 2171–2180 (2011).

[7] D. Men and M.L. Mecartney, "Superplasticity and machinability in a four-phase ceramic," *Mater. Res. Bull.*, **47** [8] 1925–1931 (2012).

[8] M. Cologna, B. Rashkova, and R. Raj, "Flash Sintering of Nanograin Zirconia in <5 s at 850°C," *J. Am. Ceram. Soc.*, **93** [11] 3556–3559 (2010).

[9] M. Cologna, A.L.G. Prette, and R. Raj, "Flash-Sintering of Cubic Yttria-Stabilized Zirconia at 750°C for Possible Use in SOFC Manufacturing," *J. Am. Ceram. Soc.*, **94** [2] 316–319 (2011).

[10] M. Cologna, J.S.C. Francis, and R. Raj, "Field assisted and flash sintering of alumina and its relationship to conductivity and MgO-doping," *J. Eur. Ceram. Soc.*, **31** [15] 2827–2837 (2011).

[11] J.A. Downs and V.M. Sglavo, "Electric Field Assisted Sintering of Cubic Zirconia at 390°C," *J. Am. Ceram. Soc.*, **96** [5] 1342–1344 (2013).

[12] H. Yoshida, Y. Sakka, T. Yamamoto, J.-M. Lebrun, and R. Raj, "Densification behaviour and microstructural development in undoped yttria prepared by flash-sintering," *J. Eur. Ceram. Soc.*, **34** [4] 991–1000 (2014).

[13] K.S. Naik, V.M. Sglavo, and R. Raj, "Field assisted sintering of ceramic constituted by alumina and yttria stabilized zirconia," *J. Eur. Ceram. Soc.*, **34** [10] 2435–2442 (2014).

[14] J.S.C. Francis and R. Raj, "Influence of the Field and the Current Limit on Flash Sintering at Isothermal Furnace Temperatures," *J. Am. Ceram. Soc.*, **96** [9] 2754–2758 (2013).

[15] S.K. Jha, J.M. Lebrun, and R. Raj, "Phase transformation in the alumina–titania system during flash sintering experiments," *J. Eur. Ceram. Soc.*, **36** [3] 733–739 (2016).

[16] K. Terauds, J.-M. Lebrun, H.-H. Lee, T.-Y. Jeon, S.-H. Lee, J.H. Je, and R. Raj, "Electroluminescence and the measurement of temperature during Stage III of flash sintering experiments," *J. Eur. Ceram. Soc.*, **35** [11] 3195–3199 (2015).

[17] R. Raj, "Joule heating during flash-sintering," *J. Eur. Ceram. Soc.*, **32** [10] 2293–2301 (2012).

[18] R. Raj, "Analysis of the Power Density at the Onset of Flash Sintering," *J. Am. Ceram. Soc.*, (2016).

[19] Y. Dong and I.-W. Chen, "Predicting the Onset of Flash Sintering," *J. Am. Ceram. Soc.*, **98** [8] 2333–2335 (2015).

[20] H. Yoshida, P. Biswas, R. Johnson, and M. Mohan, *Flash sintering of spinel JACerS paper.pdf*, (n.d.).

[21] S. Ghosh, A.H. Chokshi, P. Lee, and R. Raj, "A Huge Effect of Weak dc Electrical Fields on Grain Growth in Zirconia," *J. Am. Ceram. Soc.*, **92** [8] 1856–1859 (2009).

[22] D. Yang, R. Raj, and H. Conrad, "Enhanced Sintering Rate of Zirconia (3Y-TZP) Through the Effect of a Weak dc Electric Field on Grain Growth," *J. Am. Ceram. Soc.*, **93** [10] 2935–2937 (2010).

[23] H.Y. Akinori Uehashi, "Enhancement of sintering rates in $BaTiO_3$ by controlling of DC electric current," *J. Ceram. Soc. Jpn.*, **123** [1438] 465–468 (2015).

[24] A.C. Sutorik, C. Cooper, and G. Gilde, "Visible Light Transparency for Polycrystalline Ceramics of $MgO{\cdot}2Al_2O_3$ and $MgO{\cdot}2.5Al_2O_3$ Spinel Solid Solutions," *J. Am. Ceram. Soc.*, **96** [12] 3704–3707 (2013).

[25] National Bureau of Standards (U. S.) Monograph 259 (1971) 25

[26] B. Hallstedt, "Thermodynamic Assessment of the System $MgO–Al_2O_3$," *J. Am. Ceram. Soc.*, **75** [6] 1497–1507 (1992).

[27] R. Raj, M. Cologna, and J.S.C. Francis, "Influence of Externally Imposed and Internally Generated Electrical Fields on Grain Growth, Diffusional Creep, Sintering and Related Phenomena in Ceramics," *J. Am. Ceram. Soc.*, **94** [7] 1941–1965 (2011).

[28] S.M. Lakiza and L.M. Lopato, "Stable and Metastable Phase Relations in the System Alumina–Zirconia–Yttria," *J. Am. Ceram. Soc.*, **80** [4] 893–902 (1997).

[29] D. Pavlyuchkov, G. Savinykh, and O. Fabrichnaya, "Experimental investigation and thermodynamic modeling of the ZrO2–MgO–Al_2O_3 system," *J. Eur. Ceram. Soc.*, **34** [5] 1397–1408 (2014).

[30] T. Sasamoto, H. Hara, and T. Sata, "Mass-spectrometric Study of the Vaporization of Magnesium Oxide from Magnesium Aluminate Spinel," *Bull. Chem. Soc. Jpn.*, **54** [11] 3327–3333 (1981).

Figure Captions

Figure 1. Dilatometric curves of different applied voltages with current controlled at 25mA/mm^2.

Figure 2. Arrhenius plot of the power dissipation with different applied voltages and currents. Onset of flash sintering for pure flash sintering with 250V and 500V highlighted.

Figure 3. SEM micrographs of A) No applied E-Field, B) 50V; 25mA, C) 100V; 25mA, D) 250V; 25mA, E) 500V; 25mA, F) 250V; 75mA.

Figure 4. XRD patterns of the comparison of increasing current density.

Figure 5. XRD patterns of the spinel peak shift with increasing current density.

Figure 6. Lattice parameter as a function of atomic % Al/Mg.

Figure 7. MgO – Al_2O_3 equilibrium phase diagram. (After Hallstedt [26])

Table Captions

Table 1. Experimental parameters, calculated blackbody radiation T, density, and grain size data.

Table 2. Lattice parameters and compositions of conventionally and field assisted sintered samples listed with calculated temperatures from Table 1.

Supplementary Information Caption

S1. Video of flash sintering experiments

Tables

E-Field (V/cm)	Current (mA/mm^2)	Furnace T (°C)	Calculated Sample T (°C)	Density (%)	Avg. Grain Size (nm)
0	0	1450	1450	74	400
50	25	1430	1490	95	650
100	25	1350	1450	96	600
250	25	1230	1390	94	520
500	25	1150	1330	90	470
250	75	1230	1500	95	1500

Table 1. Experimental parameters, calculated blackbody radiation T, density, and grain size data.

Sample	8YSZ Lat. Par. (Å)	Al_2O_3 Lat. Par. (Å)	$MgAl_2O_4$ Lat. Par. (Å)	EDS Atomic Al/Mg	EDS $MgAl_2O_4$ Composition
$MgAl_2O_4$ *(1500°C, 12 h)*	------	------	a = 8.083	2.2±0.1	MgO • 1.1 Al_2O_3
3-Phase *(1500°C, 12 h)*	a = 5.142	a = 4.761 c = 12.998	a = 8.068	3.0±0.2	MgO • 1.5 Al_2O_3
0V; 0mA *(1450°C, 30s)*	a = 5.143	a = 4.759 c = 12.992	a = 8.075	------	------
50V; 25mA *(1430°C, 30s)*	a = 5.142	a = 4.760 c = 12.995	a = 8.054	2.8±0.2	MgO • 1.4 Al_2O_3
100V; 25mA *(1350°C, 30s)*	a = 5.144	a = 4.756 c = 12.994	a = 8.044	3.2±0.2	MgO • 1.6 Al_2O_3
250V; 25mA *(1230°C, 30s)*	a = 5.143	a = 4.761 c = 12.999	a = 8.031	3.6±0.2	MgO • 1.8 Al_2O_3
500V; 25mA *(1150°C, 30s)*	a = 5.136	a = 4.758 c = 12.984	a = 8.057	3.1±0.1	MgO • 1.6 Al_2O_3
250V; **75**mA *(1230°C, 30s)*	a = 5.138	------	a = 7.988	6.2±0.4	MgO • 3.1 Al_2O_3

Table 2. Lattice parameters and compositions of conventionally and field assisted sintered samples listed with calculated temperatures from Table 1.

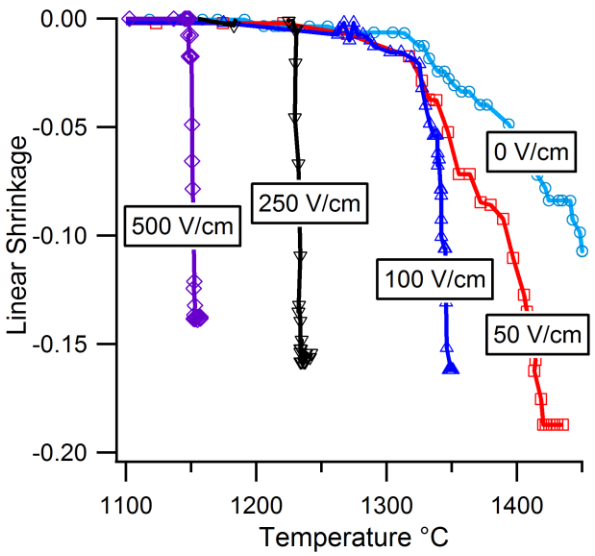

Figure 1. Dilatometric curves of different applied voltages with current controlled at 25mA/mm^2.

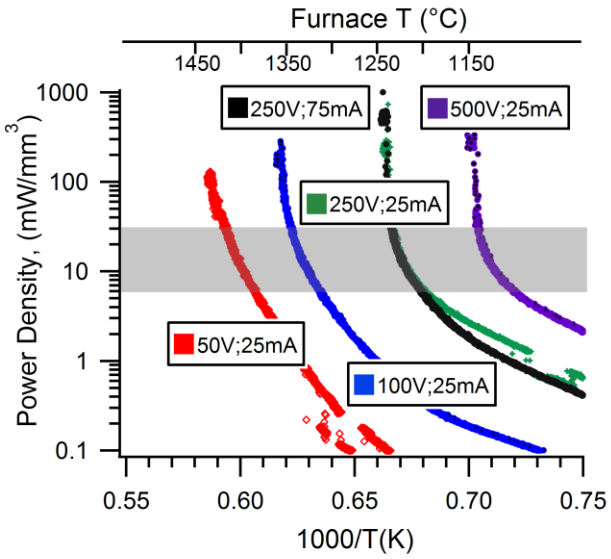

Figure 2. Arrhenius plot of the power dissipation with different applied voltages and currents.

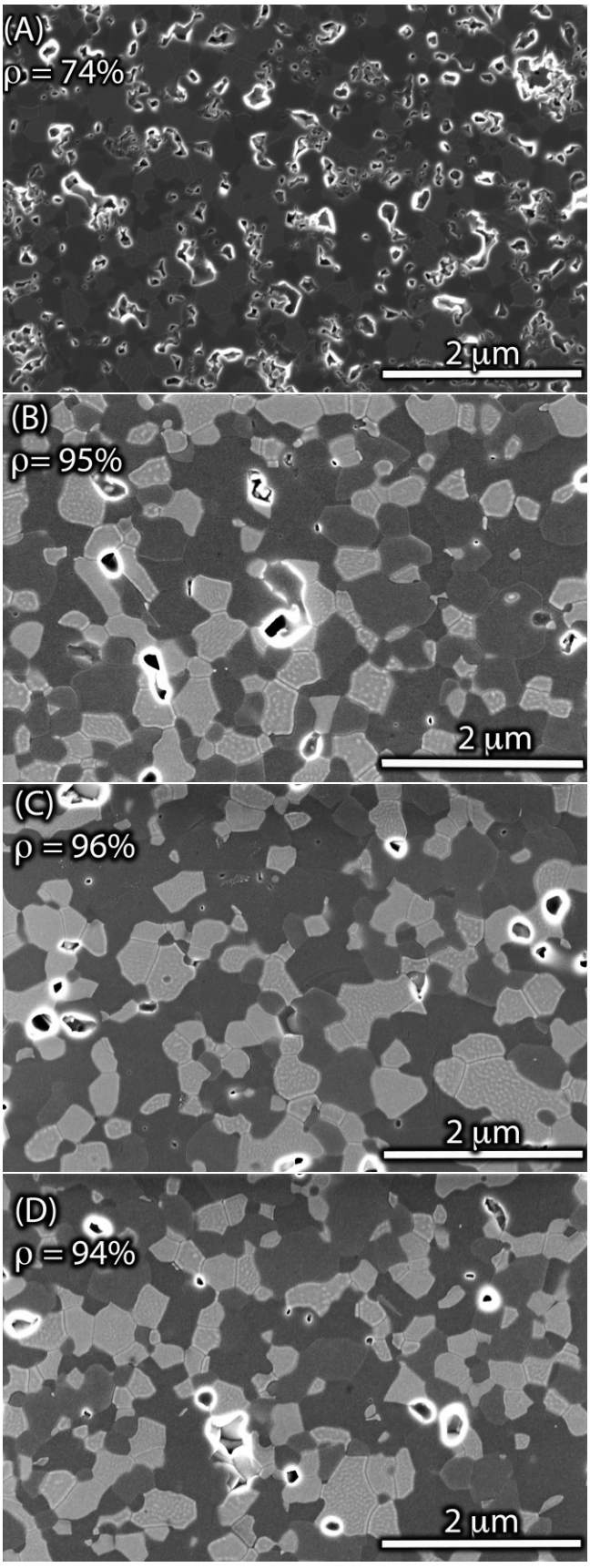
(A)
ρ = 74%
2 μm
(B)
ρ= 95%
2 μm
(C)
ρ = 96%
2 μm
(D)
ρ = 94%
2 μm

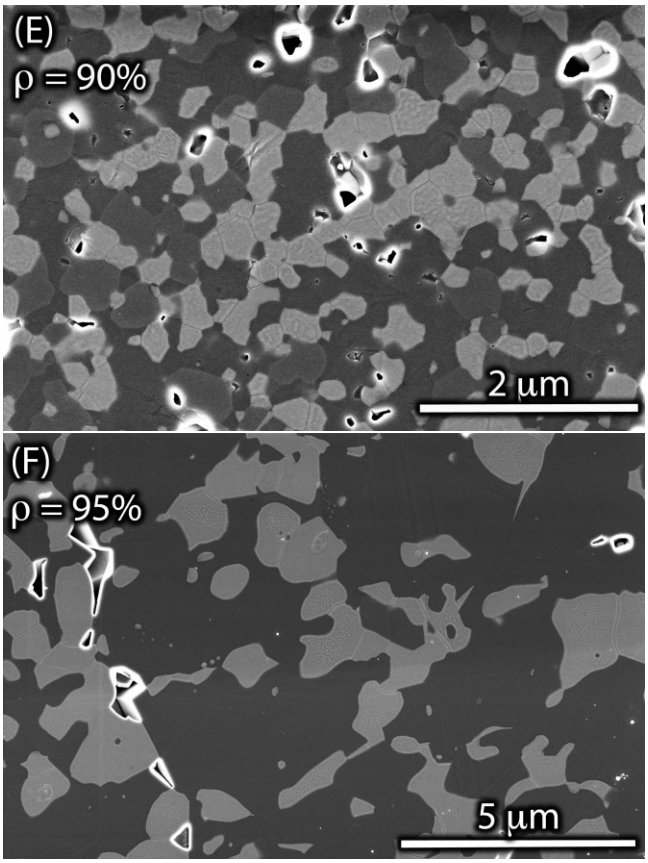

Figure 3. SEM micrographs of A) No applied E-Field, B) 50V; 25mA, C) 100V; 25mA, D) 250V; 25mA, E) 500V; 25mA, F) 250V; 75mA.

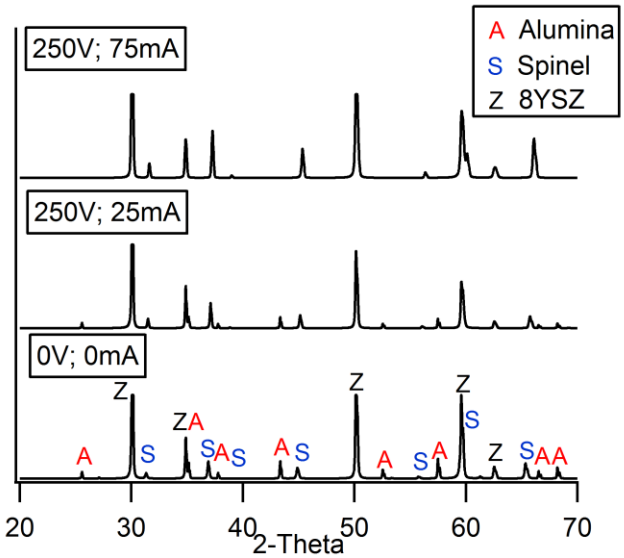

Figure 4. XRD patterns of the comparison of increasing current density.

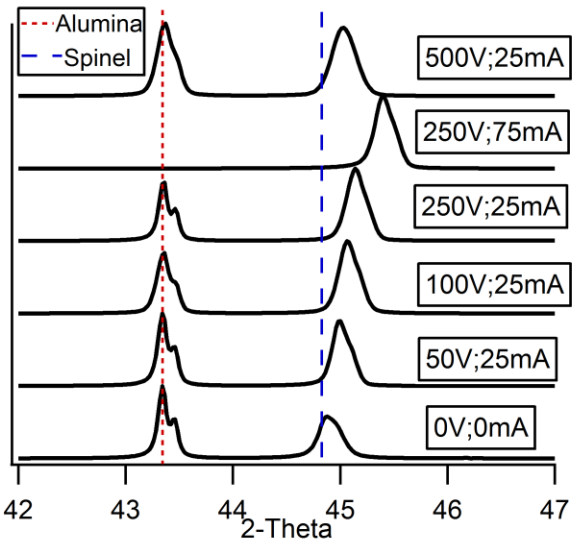

Figure 5. XRD patterns of the spinel peak shift with increasing current density.

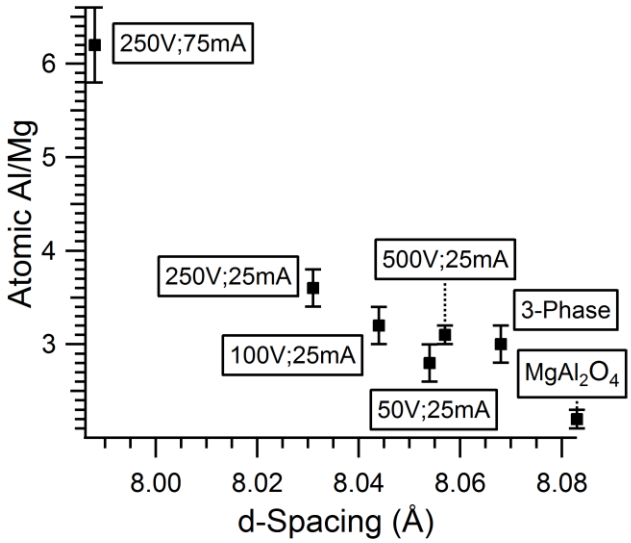

Figure 6. Lattice parameter as a function of atomic % Al/Mg.

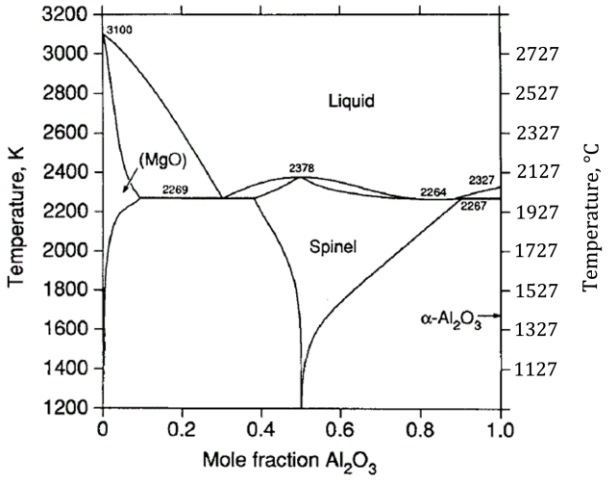

Figure 7. $MgO - Al_2O_3$ equilibrium phase diagram. (After Hallstedt [25])